Bull. Mater. Sci., Vol. 6, No. 2, May 1984, pp. 369–393. © Printed in India.

Structural disorder and solid state transformations in single crystals of $Zn_xCd_{1-x}S$ and $Zn_xMn_{1-x}S$

M T SEBASTIAN and P KRISHNA

Physics Department, Banaras Hindu University, Varanasi 221 005, India

Abstract. Single crystals of $Zn_xCd_{1-x}S$ and $Zn_xMn_{1-x}S$ were grown from the vapour phase at 1100°C in the range $x = 0{\cdot}9$ to 1. X-ray characterization shows that polytypes and disordered structures occur in $Zn_xCd_{1-x}S$ for $x \geqslant 0{\cdot}94$, whereas $Zn_xMn_{1-x}S$ displays disordered and polytype structures in the entire range $x = 0{\cdot}9$ to 1. It is observed that $Zn_xCd_{1-x}S$ and $Zn_xMn_{1-x}S$ undergo a 2H–6H solid state transformation on annealing in vacuum around 600°C. Experimental analysis of the intensity distribution along the $10{\cdot}L$ reciprocal lattice row as recorded on a single crystal diffractometer from partially transformed crystals shows that the mechanism of the transformation cannot be explained in terms of the one-parameter models of non-random faulting reported earlier. A two-parameter theoretical model with α representing the probability of random insertion of a fault in the 2H structure and β representing the probability of the growth of the 6H nucleus, is developed both for a deformation mechanism and a layer displacement mechanism. It is found that the theoretical model of non-random deformation faulting with $\beta \gg \alpha$ approximates the actual mechanism of transformation in these crystals.

Keywords. Structural disorder; single crystals; polytype structures; theoretical models.

1. Introduction

In recent years there has been considerable interest in the study of mixed crystals of the type $Zn_xCd_{1-x}S$ and $Zn_xMn_{1-x}S$ and the characterization of their physical properties. The possibility of obtaining a systematic variation of photoelectronic properties simply by adjusting the solid solution composition has given rise to an interest in optoelectronic applications of $Zn_xCd_{1-x}S$ crystals, mainly luminescence applications (Brodin *et al* 1970; Kawaguchi *et al* 1976; Yoshikawa and Sakai 1976) and heterojunctions for photovoltaic energy conversion (Burton and Hench 1976; Domeus *et al* 1977). Manganese-doped ZnS (ZnS : Mn) provides an efficient system for high field electroluminescence (Theis 1981) and the electroluminescent devices exhibit (Inouguchi *et al* 1974) characteristics which are especially attractive for use in flat panel refreshed matrix displays with high peak luminescence-voltage response. Such devices can be operated (Inouguchi *et al* 1974) at high brightness for tens of thousands of hours at constant voltage with little loss of luminescence.

It is therefore of considerable interest to examine the defects present in such crystals and study their influence on device properties. It is well known that single crystals of ZnS when grown from the vapour phase at temperatures above 1050°C show a variety of polytype structures with considerable random disorder. On the other hand CdS which is isostructural with ZnS does not exhibit polytype structures and the related disorder effects (Chandrasekharaiah and Krishna 1969). Zinc sulphide and cadmium sulphide both display two polymorphic structures—wurtzite (2H) and sphalerite (3C).

Manganese sulphide on the other hand exists in three polymorphic forms—a stable green α-MnS with the rock salt structure and two pink metastable adamantine structures β-MnS (sphalerite type) and γ-MnS (wurtzite type). The β and γ-forms are metastable at room temperature and convert (Mehmed and Heraldson 1938; Schnaase 1933) into α-MnS on heating at 200°C. β-MnS is also known to convert into α-MnS at high pressure (Roomians 1963).

CdS and ZnS are known to form solid solutions of the type $Zn_xCd_{1-x}S$ for all values of x (Cherin *et al* 1970). MnS and ZnS on the other hand form a continuous series of solid solutions only in the range $x = 0$ to 0·52 (Schnaase 1933; Kröger 1939; Juza *et al* 1956; Lutz and Becker 1977). The present investigation was undertaken to study (i) the variation of the disorder effects in single crystals of $Zn_xCd_{1-x}S$ and $Zn_xMn_{1-x}S$ with change of composition and (ii) the effect of composition on the wurtzite-sphalerite (2H-3C) phase transformation which is known to give rise to defect structures in these materials.

2. Crystal growth, characterization and annealing behaviour of $Zn_xCd_{1-x}S$

Single crystals of $Zn_xCd_{1-x}S$ $(1 > x > 0{\cdot}90)$ were grown (Sebastian and Krishna 1983) from the vapour phase at 1100°C in the presence of H_2S gas. Needle-shaped crystals ranging in length from 0·5–8 mm and in width from 0·1–0·5 mm were obtained. For $x = 0{\cdot}95$ we observed dendritic growth with large sword-shaped dendrites branching and rebranching at 60° angles as seen in figure 1(a). The $Zn_{0{\cdot}95}Cd_{0{\cdot}05}S$ dendrites grew as needles along the $\langle 10\bar{1}0 \rangle$ directions and finally merged to form a platelet perpendicular to [0001]. Figure 1 shows the dendrites at four different stages of growth.

The structure of as-grown $Zn_xCd_{1-x}S$ crystals was examined (Sebastian and Krishna 1983) by x-ray diffraction by recording 15° c-axis oscillation photographs. The crystals showed different structures depending on the amount of cadmium present in the crystal. All the crystals with a composition $x \leqslant 0{\cdot}93$ were free of stacking faults and had a perfect 2H structure. For $x \geqslant 0{\cdot}94$ the crystals were found to contain 2H, 3C, 2H + 3C, polytype and disordered structures. The dendrites observed at $x = 0{\cdot}95$ were single crystals containing 2H + 3C + disorder in their structure.

Needle-shaped crystals of 2H $Zn_xCd_{1-x}S$ were annealed in vacuum at successively higher temperatures in the range 400–1100°C for 1 hr each and then quenched in cold water to arrest the structural transformations induced in them. During annealing the crystals were kept immersed in ZnS powder in a silica tube to prevent the crystal from vapourising at high temperatures. After each annealing run the crystals were quenched by immersing the silica tube in cold running water. The structure of the crystals was re-examined by x-ray diffraction after each annealing followed by quenching. The crystals were also examined under an optical microscope before and after annealing to detect any macroscopic kinks characteristic of crystals undergoing transformation by the periodic slip mechanism.

It is found that the transformation behaviour of the 2H $Zn_xCd_{1-x}S$ crystals depends on the value of x. The crystals with the composition $x > 0{\cdot}98$ transformed to a disordered twinned 3C structure in a manner similar to that reported earlier for ZnS (Sebastian *et al* 1982, 1983a). The 2H crystals in the composition range $0{\cdot}98 > x > 0{\cdot}95$ on annealing transformed to a disordered 6H structure around 600°C.

Figure 1. Optical micrographs showing the progress of dendritic growth of $Zn_{0.95}Cd_{0.05}S$ crystals. The axis of the dendrites is found to be along $[10\bar{1}0]$ with the c-axis nearly perpendicular to the plane of the figure. The dendrites appear to merge into a platelet as the growth proceeds (× 20).

These crystals on further annealing, at higher temperatures transformed to a disordered twinned 3C structure around 800°C. The crystals in the range $0{\cdot}95 \geqslant x > 0{\cdot}93$ behave differently. Nearly 30% of the crystals studied transformed to a

disordered 6H structure and the rest to a disordered 2H structure around 600°C. These crystals on further annealing at higher temperatures do not transform to a 3C structure. Figure 2 shows the $10 \cdot L$ reciprocal lattice row of a $Zn_{0.94}Cd_{0.06}S$ crystal before and after annealing at 800°C. The crystals with $x < 0.93$ do not undergo any structural transformation and remain as perfect 2H in the temperature range up to 1100°C indicating that the addition of CdS to ZnS stabilizes the 2H phase in the solid solution.

3. Growth, characterization and annealing behaviour of $Zn_xMn_{1-x}S$ crystals

Single crystals of $Zn_xMn_{1-x}S$ were grown in a manner similar to that described for $Zn_xCd_{1-x}S$. Polycrystalline ZnS and MnS were mixed in calculated proportions for different values of x ($0.9 \leqslant x < 1$). The crystals obtained were needle-shaped, up to 5 mm in length and 1 mm thick. The crystals were examined by x-ray diffraction and were found to contain perfect 2H, disordered 2H, 2H + 3C, polytypes and disordered structures. The 6H structure was encountered more frequently than in $Zn_xCd_{1-x}S$ crystals.

Needle-shaped crystals of $Zn_xMn_{1-x}S$ were annealed in vacuum in the temperature range 400–1100°C for 1 hr each and quenched in the manner described earlier for $Zn_xCd_{1-x}S$ crystals. The structure of the crystals was re-examined by x-ray diffraction after each annealing run. It was observed that nearly 75% of the 2H $Zn_xMn_{1-x}S$ crystals transformed to a disordered twinned 3C structure in a manner similar to that observed for pure ZnS (Sebastian *et al* 1982). In the remaining 25% crystals disordered 6H structure was observed around 500°C as an intermediate state. On further annealing at higher temperatures this disordered 6H structure transformed to a

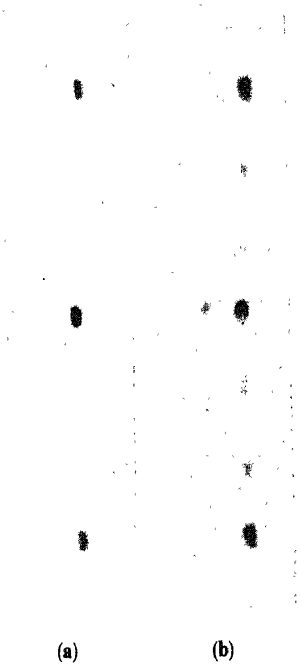

Figure 2. The $10.L$ reciprocal lattice row of a 2H $Zn_{0.93}Cd_{0.07}S$ crystal recorded (a) before annealing (b) after annealing at 800°C for 1 hr. The crystal has transformed partially to a 6H structure. (Camera radius 3 cm, CuK radiation × 4).

(a) (b)

Figure 3. The 10.L reciprocal lattice row of a 2H $Zn_{0.9}Mn_{0.1}S$ crystal recorded (a) before annealing (b) after annealing at 600°C for 1 hr. The 2H reflections have nearly disappeared and diffuse reflections have developed in positions of 3C and 6H reflections. (Camera radius 3 cm, CuK radiation. × 3).

disordered twinned 3C structure. All the crystals transformed back to a disordered 2H structure on annealing above 1050°C. Figure 3 shows the $10 \cdot L$ row of a perfect 2H $Zn_{0.9}Mn_{0.1}S$ crystal before and after annealing at 600°C for 1 hr. Most of the crystals which transformed to the twinned 3C structure showed an enhancement of intensity at positions of 6H reflections along the $10 \cdot L$ row. After each annealing run the crystals were examined under an optical microscope to detect any change in the shape of the crystals. No kinks or other macroscopic changes in the shape of the crystals were observed after transformation.

4. Mechanism of the 2H-6H transformation

Daniels (1966) and Mardix and Steinberger (1966) proposed a periodic slip mechanism to explain the 2H-3C transformation in ZnS and for the formation of long period polytypes. This envisages the expansion of stacking faults around an axial screw dislocation causing them to occur with a period equal to the Burgers vector of the screw dislocation. However, periodic slip caused by the expansion of a single deformation fault around a screw dislocation of 6 layered Burgers vector in a 2H structure would give rise to an 18R structure as shown below

initial structure:

$$\begin{aligned} &ABABAB|ABABABABABABABABAB\ldots\ldots \\ &\qquad CACACA|CACACACACACACA\ldots\ldots \\ &\qquad\qquad BCBCBC|BCBCBC\ldots\ldots \\ &\qquad\qquad\qquad ABABAB|\ldots\ldots \end{aligned}$$

resulting structure:

$$ABABABCACACABCBCBCABABAB\ldots\ldots = 18R\ (1113)_3$$

The transformation to a 6H structure is only possible if two partial dislocations of opposite signs occur at three layer separations and expand simultaneously around a screw dislocation of 6-layered Burgers vector. Moreover, crystals undergoing a 2H-6H transformation by the periodic slip mechanism should develop macroscopic kinks. The absence of such kinks and the strong diffuse intensity observed on x-ray diffraction photographs along the $10 \cdot L$ reciprocal lattice row indicate that the transformation has occurred by the non-random nucleation of stacking faults at three-layer separations (Secco d'Aragona *et al* 1966; Sebastian *et al* 1982). In this case the Burgers vector of the partial dislocation bounding each stacking fault can be in any of three symmetry related directions. Since each fault nucleates independently, the three directions would occur with equal probability producing no macroscopic kinks. Even in crystals which do not contain a screw dislocation, the faults can nucleate preferentially at 3-layer separations in order to effect the 2H-6H transformation. A similar transformation from the 2H to the 6H structure has been observed earlier by Krishna and Marshall (1971) in SiC and possible mechanisms were investigated in detail by Pandey *et al* (1980).

4.1 *Theoretical models*

The 2H to 6H transformation in close-packed structures can occur by two different mechanisms involving the non-random insertion of either layer displacement faults or deformation faults (Pandey *et al* 1980) in the 2H structure. If layer displacement faults nucleate at three-layer separations the 2H structure would convert to a 6H structure as shown below

initial structure: $AB\underline{A}BAB\underline{A}BAB\underline{A}BAB\ldots\ldots$

resulting structure: $ABC\underline{B}AC\underline{A}BC\underline{B}AC\underline{A}BAB\ldots\ldots$

The layers indicated by underlining have changed their positions. The same transformation can also be effected by the insertion of deformation faults at three layer separations as depicted below

initial structure: $AB|ABABABABAB\ldots\ldots$

$CAC|ACACACA\ldots\ldots$

$BAB|ABAB\ldots\ldots$

$CAC|A\ldots\ldots$

$B\ldots\ldots$

resulting structure: $ABCACBABCACB\ldots\ldots$

Pandey *et al* (1980) have theortically calculated the diffraction effects that would be expected from crystals undergoing transformation by both the mechanisms on the assumption that faults do not occur at less than three layer separations but otherwise have the same probability of occurrence at all layers. On the basis of this one-parameter model the main differences in the diffraction effects expected from crystals undergoing

2H-6H transformation by the layer displacement and deformation mechanisms are as follows

(i) The reflections $H-K \neq 3n$ and $L = 0, \pm 1$ (mod 2) of the 2H structure remain sharp and unbroadened throughout the transformation for the layer displacement mechanism while these are considerably broadened for transformation by the deformation mechanism

(ii) For transformation by the layer displacement mechanism a diffuse reflection develops initially around the position $L = \pm\frac{1}{2}$ (mod 2) and then splits into two reflections which migrate towards the $L = \pm\frac{1}{3}$ (mod 2) and $L = \pm\frac{2}{3}$ (mod 2) positions as the transformation proceeds towards 6H. At an intermediate stage of transformation the new 6H reflections are thus shifted towards each other *i.e.*, towards the $L = \pm\frac{1}{2}$ (mod 2) position. For transformation by the deformation mechanism, the new reflections characteristic of the 6H structure appear initially near positions $L = \pm\frac{1}{6}, \pm\frac{5}{6}$ (mod 2) and then approach towards $L = \pm\frac{1}{3}, \pm\frac{2}{3}$ (mod 2) as the transformation progresses towards the 6H structure. At an intermediate stage of transformation these reflections are thus shifted away from each other *i.e.*, away from the $L = \pm\frac{1}{2}$ (mod 2) positions.

Therefore the nature of stacking faults involved in the structural transformation can be determined by studying the peak broadening and peak shifts of x-ray diffraction maxima recorded from partially transformed crystals.

4.2 *Analysis of the observed intensity profiles and comparison with the one-parameter model*

The point intensity distribution along the $10 \cdot L$ reciprocal lattice row of several partially transformed crystals in different stages of transformation was recorded on a four-circle computer-controlled single crystal diffractometer using the method described earlier by Pandey and Krishna (1977). MoKα radiation was used to record the intensity diffracted by the crystal. The crystal and the counter were held stationary during each observation and the crystal was oriented by the computer to diffract the $10 \cdot L$ row for different values of L (in steps of $\Delta L = 0{\cdot}01$) into the counter. The divergence of the incident beam was adjusted to cover the mosaic spread in the crystal. The sharp reflections $H - K = 0$ (mod 3) were used to orient the crystal and to define the hexagonal unit cell. Figure 4 shows the diffractometer record of intensity along the $10 \cdot L$ reciprocal lattice row as recorded from a 2H $Zn_{0{\cdot}93}Cd_{0{\cdot}07}S$ crystal after annealing at 800°C for 1 hr. The crystal is in the initial stage of transformation and the 6H peaks have just begun to appear. The 2H reflections are quite sharp and the new 6H reflections are shifted from their correct positions. Figure 5 shows a similar intensity record obtained from a $Zn_{0{\cdot}94}Cd_{0{\cdot}06}S$ crystal at a more advanced stage of the 2H-6H transformation. The 6H peaks are more clearly developed and are much less shifted from their correct positions. Similar diffractometer records were obtained on annealing 2H crystals of $Zn_xMn_{1-x}S$ at different stages of transformation. The intensity profiles obtained experimentally from partially-transformed crystals show that the new 6H reflections appear at an earlier stage of transformation and are shifted in the direction predicted by the deformation mechanism. However, the 2H and 6H peaks are much sharper than what is expected on the basis of the one-parameter model and the shift of

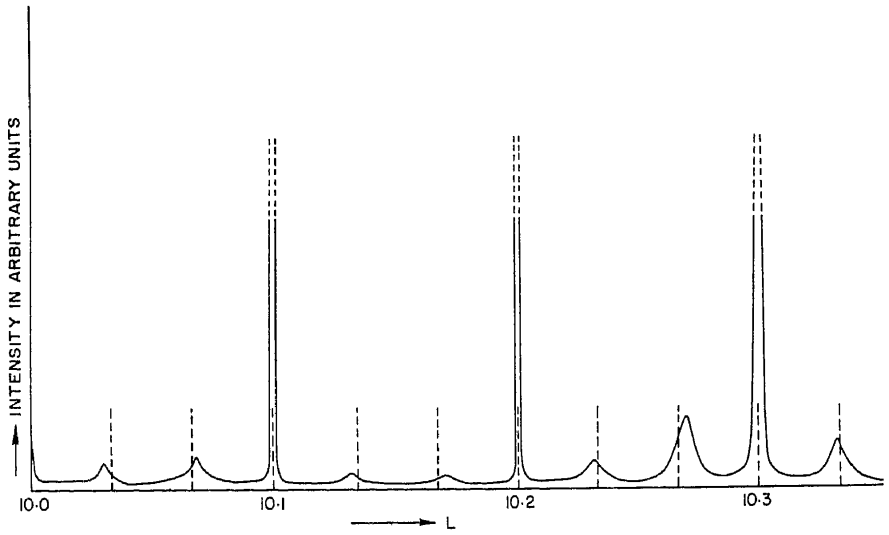

Figure 4. Single crystal diffractometer plot of intensity versus L along the $10 \cdot L$ reciprocal lattice row recorded after annealing a perfect 2H $Zn_{0.93}Cd_{0.07}S$ crystal at 800°C for 1 hr. Vertical dashed lines indicate the correct 6H positions from which the new 6H peaks are clearly shifted. The 2H peaks are very sharp and intense and the crystal is in an early stage of transformation.

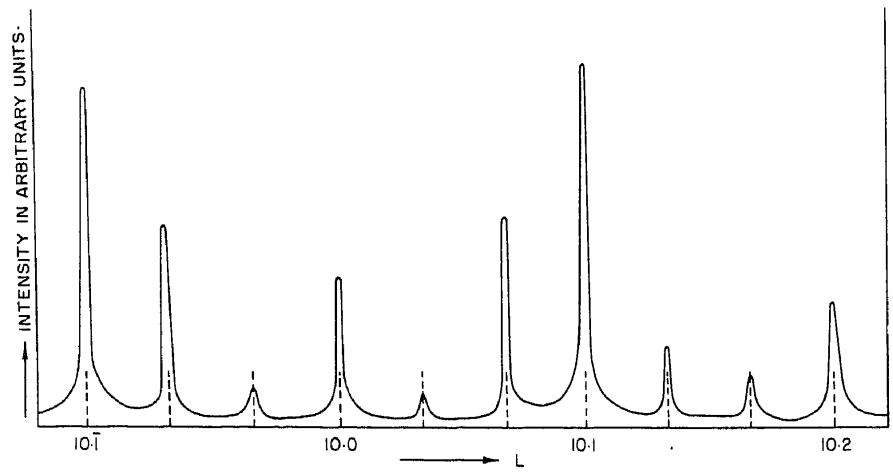

Figure 5. Single crystal diffractometer plot of intensity versus L along the $10 \cdot L$ reciprocal lattice row recorded after annealing a perfect 2H crystal of $Zn_{0.94}Cd_{0.06}S$ at 800°C for 1 hr. Vertical dashed lines indicate the correct 6H positions. The crystal is at a more advanced stage of transformation.

the 6H reflections is also much smaller. Therefore it is evident that the 2H-6H transformation in $Zn_xCd_{1-x}S$ and $Zn_xMn_{1-x}S$ crystals does not take place in accordance with the one-parameter model proposed by Pandey *et al* (1980).

5. Development of a two-parameter model

From the experimental results described above it appears that the probability (β) of faults nucleating at 3-layer separations is much larger than the probability (α) of their occurrence at larger separations. The former (β) corresponds to the probability of the growth of a 6H nucleus within the 2H phase and the latter (α) to the probability of fresh nucleation of a fault in the 2H structure. It is possible to develop the theory of x-ray diffraction from 2H crystals undergoing transformation to the 6H structure by (i) the deformation mechanism and (ii) the layer displacement mechanism using two parameter model. A choice between the two mechanisms can then be made from a comparison of the theoretically-predicted diffraction effects with those actually observed provided only one of the mechanisms is operative in the crystal at a time. The need for a two parameter model for ZnS was recognized by Jagodzinski (1949), Müller (1952) and Singer (1963). More recently Lele and Pandey (1982) employed a 2-parameter model to theoretically investigate the 3C–2H transformation in cobalt.

We develop below the theory of x-ray diffraction from crystals undergoing the 2H-6H solid state transformation by (i) the deformation mechanism and (ii) the layer displacement mechanism under the following assumptions:

(i) The crystal is infinite in size and free of distortions.
(ii) The scattering power for all the layers is the same.
(iii) There is no change in the layer spacings at the faults.
(iv) The faults extend right across the crystal boundaries.
(v) The faults occur preferentially at 3-layer separations with a fault probability β which is different from the probability α of random nucleation at larger separations. The probability of faults occurring at less than 3 layer separations is negligible.

5.1 *The theory of x-ray diffraction from crystals undergoing the 2H–6H solid state transformation by the deformation mechanism*

In the perfect 2H structure we distinguish two types of layers with subscripts 0 and 1 according as the stacking offset vector is $+S_i$ or $-S_i$ where S_i denotes $S_1 = \frac{1}{3}a\,[1\bar{1}00]$, $S_2 = \frac{1}{3}a\,[01\bar{1}0]$ and $S_3 = \frac{1}{3}a\,[\bar{1}010]$. The perfect 2H structure can thus be written as

$$A_0B_1A_0B_1A_0B_1A_0B_1 \ldots .$$

There are six other types of layers in a 2H crystal undergoing transformation to the 6H structure by the deformation mechanism. Let the subscripts 0^1 and 1^1 denote the first layer of the slipped stack according as it follows a 0 type or 1 type layer. It is assumed that the next two layers after a 0^1 or 1^1 type layer are unfaulted. Therefore the layer following a 0^1 or 1^1 layer is designated as 0^2 or 1^2. The next layer after this is denoted as 0^3 or 1^3 in order to distinguish it from 0 or 1, since there is a probability β that the growth of a 6H nucleus may commence from these layers. We can now compute the probability $P_{(m,j)}$ of arriving at the mth layer with the subscript j ($j = 0, 1, 0^1, 1^1, 0^2, 1^2, 0^3$ and 1^3) with the help of the following probability trees which consider the

transitions from $(m-1)$th layer to the mth layer with each type of layer at the origin (Sebastian and Krishna 1983b):

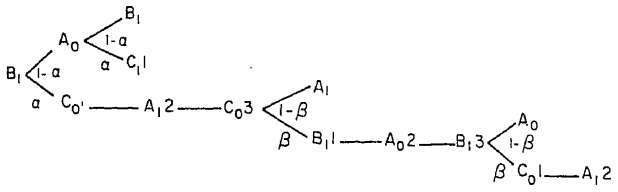

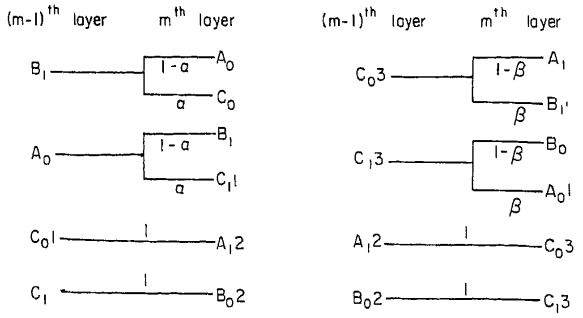

As shown in the probability trees, the layer type following B_1 (or A_0) layers in the absence of a deformation fault is A_0 (or B_1) and occurs with the probability $(1-\alpha)$. Therefore in the presence of a deformation fault the layer following B_1 (or A_0) is C_{0^1} (or C_{1^1}).

The probability $P_{(m,j)}$ may now be computed as follows

$$P_{(m,0)} = (1-\alpha)P_{(m-1,1)} + (1-\beta)P_{(m-1,1^3)}, \tag{1}$$

$$P_{(m,1)} = (1-\alpha)P_{(m-1,0)} + (1-\beta)P_{(m-1,0^3)}, \tag{2}$$

$$P_{(m,0^1)} = \alpha P_{(m-1,1)} + \beta P_{(m-1,1^3)}, \tag{3}$$

$$P_{(m,1^1)} = \alpha P_{(m-1,0)} + \beta P_{(m-1,0^3)}, \tag{4}$$

$$P_{(m,0^2)} = P_{(m-1,1^1)}, \tag{5}$$

$$P_{(m,1^2)} = P_{(m-1,0^1)}, \tag{6}$$

$$P_{(m,0^3)} = P_{(m-1,1^2)}, \tag{7}$$

$$P_{(m,1^3)} \; P_{(m-1,0^2)}. \tag{8}$$

The function $J_{(m,j)}$ can be written (Prasad and Lele 1971) as

$$J_{(m,j)} = \exp(i\phi_m)_j = \sum P_{(m,j)} \exp(i\phi_m)_j, \tag{9}$$

where

$$\exp(i\phi_m) = \exp(i\phi_{m-1})\exp(\pm i\phi_0), \tag{10}$$

and $\phi_0 = 2\pi/3$ is the phase difference between the $(m-1)$th and mth layers and takes plus or minus sign depending on the layer sequence being cyclic $A \to B \to C \to A$ or anticyclic $A \to C \to B \to A$. Using (1) to (10) and putting

$$\exp(+i\phi_0) = \omega_1 \text{ and } \exp(-i\phi_0) = \omega_2$$

we get

$$J_{(m,0)} = (1-\alpha)J_{(m-1,1)}\omega_2 + (1-\beta)J_{(m-1,1^3)}\omega_2, \tag{11}$$

$$J_{(m,1)} = (1-\alpha)J_{(m-1,0)}\omega_1 + (1-\beta)J_{(m-1,0^3)}\omega_1, \tag{12}$$

$$J_{(m,0^1)} = \alpha J_{(m-1,1)}\omega_1 + \beta J_{(m-1,1^3)}\omega_1, \tag{13}$$

$$J_{(m,1^1)} = \alpha J_{(m-1,0)}\omega_2 + \beta J_{(m-1,0^3)}\omega_2, \tag{14}$$

$$J_{(m,0^2)} = J_{(m-1,1^1)}\omega_2, \tag{15}$$

$$J_{(m,1^2)} = J_{(m-1,0^1)}\omega_1, \tag{16}$$

$$J_{(m,0^3)} = J_{(m-1,1^2)}\omega_2, \tag{17}$$

$$J_{(m,1^3)} = J_{(m-1,0^2)}\omega_1. \tag{18}$$

Let the solution of the system of difference equations (11) to (18) be of the form

$$J_{(m,j)} = C_j \rho^m, \qquad m \geqslant 0, \tag{19}$$

where C_j and ρ are functions of α and β. Substituting in equations (11) to (18) and eliminating the various C's we finally get the so-called characteristic equation

$$\rho^8 - (1-\alpha)^2\rho^6 + \alpha(1-\beta)\rho^4 - \beta^2\rho^2 + (\alpha^2 + \beta^2 - 2\alpha\beta) = 0. \tag{20}$$

Holloway (1969) obtained an analytic solution for the diffracted intensity in terms of coefficients and boundary conditions of the characteristic equation. His intensity expression is

$$I = f^2 C\left[\left(\frac{1}{2} + \frac{\sum_{j=1}^{n-1}\sum_{k=0}^{j-1} a_{n-k}T_{j-k}\exp(n-j)i\pi L - a_0}{\sum_{j=0}^{n} a_j \exp(ji\pi L)}\right) + \text{C.C.}\right], \tag{21}$$

where a_n is the coefficient of ρ^n in the characteristic equation, T's are the boundary conditions, C is a scale factor and

$$f^2 = f_{Zn}^2 + f_S^2 + 2f_{Zn}f_S\cos\frac{3\pi L}{4}.$$

In the present case

$$n = 8,\ a_8 = 1,\ a_6 = -(1-\alpha)^2,\ a_4 = \alpha(1-\beta),$$
$$a_2 = -\beta^2 \text{ and } a_0 = (\alpha-\beta)^2,$$
$$a_7 = a_5 = a_3 = a_1 = 0.$$

The boundary conditions (T's) can be found out by the following method. First we find the probability W_j of finding a layer with subscript j on passing through an arbitrary region of the crystal. From the probability tree we get

$$W_0 = (1-\alpha)W_1 + (1-\beta)W_{1^3},$$
$$W_1 = (1-\alpha)W_0 + (1-\beta)W_{0^3},$$
$$W_{0^1} = \alpha W_1 + \beta W_{1^3} = W_{1^2} = W_{0^3},$$
$$W_{1^1} = \alpha W_0 + \beta W_{0^3} = W_{0^2} = W_{1^3},$$
$$W_0 + W_1 + W_{0^1} + W_{1^1} + W_{0^2} + W_{1^2} + W_{0^3} + W_{1^3} = 1.$$

Solving the above equations we get

$$W_0 = W_1 = \frac{1-\beta}{2-2\beta+6\alpha} \tag{22}$$

$$W_{0^1} = W_{1^1} = W_{0^2} = W_{1^2} = W_{0^3} = W_{1^3} = \frac{\alpha}{2-2\beta+6\alpha}. \tag{23}$$

The boundary condition (which is the sum of the product of the phase factor and the probability factor from all the origins) can now be obtained by considering all possible sequences starting with layers of each type 0, 1, 0^1, 1^1, 0^2, 1^2, 0^3 and 1^3 at the origin and writing T_m in each case *i.e.*,

$$T_m = \sum_j W_j \langle \exp(i\phi_m)_j \rangle .$$

Thus

$$T_1 = -\tfrac{1}{2}, \qquad T_2 = \frac{2-2\beta}{2(1-\beta+3\alpha)},$$

$$T_3 = -\frac{1-\beta.}{2(1-\beta+3\alpha)}, \qquad T_4 = \frac{(1-3\alpha)(1-\beta)}{1-\beta+3\alpha},$$

$$T_5 = -\frac{1-3\alpha-\beta-3\alpha^2+6\alpha\beta+3\alpha^2\beta}{2(1-\beta+3\alpha)},$$

$$T_6 = \frac{2-12\alpha-2\beta+12\alpha^2+18\alpha\beta-6\alpha^3-12\alpha^2\beta+6\alpha^3\beta}{2(1-\beta+3\alpha)},$$

$$T_7 = -\frac{1-6\alpha-\beta+3\alpha^2+12\alpha\beta-3\alpha^2\beta-3\alpha\beta^2-3\alpha^4+3\alpha^4\beta}{2(1-\beta+3\alpha)}.$$

Substituting the coefficients (a's) and the seven boundry conditions(T's) in (21) and carrying out the summations we get the intensity expression as

$$\begin{aligned} I = f^2C\{[\tfrac{1}{2} &+ (T_1\exp(7i\pi L)+T_2\exp(6i\pi L)+(T_3+a_6T_1)\exp(5i\pi L) \\ &+ (T_4+a_6T_2)\exp(4i\pi L)+(T_5+a_6T_3+a_4T_1)\exp(3i\pi L) \\ &+ (T_6+a_6T_4+a_4T_2)\exp(2i\pi L)+(T_7+a_6T_5+a_4T_3+a_2T_1) \\ &\times \exp(i\pi L)-a_0)/(a_0+a_2\exp(2i\pi L) \\ &+ a_4\exp(4i\pi L)+a_6\exp(6i\pi L)+\exp(8i\pi L))]+\text{C.C.}\}. \end{aligned} \tag{24}$$

On simplifying (24) we get the final intensity expression for a 2H crystal undergoing solid state transformation to the 6H structure as

$$I = f^2C\left(1+\frac{x}{y}\right), \tag{25}$$

where

$$\begin{aligned} x = {} & B_1R_1+a_0B_1R_7+a_2B_1R_5+a_4B_1R_3+a_6B_1R_1+ \\ & B_2R_2+a_0B_2R_6+a_2B_2R_4+a_4B_2R_2+a_6B_2+ \\ & B_3R_3+a_0B_3R_5+a_2B_3R_3+a_4B_3R_1+a_6B_3R_1+ \\ & B_4R_4+a_0B_4R_4+a_2B_4R_2+a_4B_4+a_6B_4R_2+ \end{aligned}$$

$$B_5R_5 + a_0B_5R_3 + a_2B_5R_1 + a_4B_5R_1 + a_6B_5R_3 +$$
$$B_6R_6 + a_0B_6R_2 + a_2B_6 + a_4B_6R_2 + a_6B_6R_4 +$$
$$B_7R_7 + a_0B_7R_1 + a_2B_7R_1 + a_4B_7R_3 + a_6B_7R_5 +$$
$$B_8R_8 + a_0B_8 + a_2B_8R_2 + a_4B_8R_4 + a_6B_8R_6.$$

$$y = G_1 + G_2R_2 + G_3R_4 + G_4R_6 + G_5R_8 + G_6R_2$$
$$+ G_7R_4 + G_8R_6 + G_9R_2 + G_{10}R_4 + G_{11}R_2$$

$$B_1 = 2T_1, \quad B_2 = 2T_2, \quad B_3 = 2(T_3 + a_6T_1), \quad B_4 = 2(T_4 + a_6T_2),$$
$$B_5 = 2(T_5 + a_6T_3 + a_4T_1), \quad B_6 = 2(T_6 + a_6T_4 + a_4T_2),$$
$$B_7 = 2(T_7 + a_6T_5 + a_4T_3 + a_2T_1), \quad B_8 = -2a_0,$$

$$R_1 = \cos \pi L, \quad R_2 = \cos 2\pi L, \quad R_3 = \cos 3\pi L,$$
$$R_4 = \cos 4\pi L, \quad R_5 = \cos 5\pi L, \quad R_6 = \cos 6\pi L,$$
$$R_7 = \cos 7\pi L, \quad R_8 = \cos 8\pi L,$$

$$G_1 = 1 + a_0^2 + a_2^2 + a_4^2 + a_6^2, \quad G_2 = 2a_2a_0,$$
$$G_3 = 2a_0a_4, \quad G_4 = 2a_0a_6, \quad G_5 = 2a_0, \quad G_6 = 2a_2a_4,$$
$$G_7 = 2a_2a_6, \quad G_8 = 2a_2, \quad G_9 = 2a_4a_6, \quad G_{10} = 2a_4, \quad G_{11} = 2a_6.$$

5.1a *Prediction of diffraction effects.* The variation of the diffracted intensity with $L(h_3)$ along the $10 \cdot L$ reciprocal lattice row for different values of α and β as calculated from (25) in steps of $\Delta L = 0{\cdot}01$ are depicted in figure 6a, b, c, d, e and f. The x-ray diffraction effects from a 2H crystal undergoing transformation to the 6H structure by the deformation mechanism are as follows

(i) Reflections with $H - K = 0 \pmod 3$ and $L = 0 \pmod 2$ are unaffected by the transformation and remain sharp throughout the transformation.

(ii) The following diffraction effects are predicted for reflections with $H - K \neq 0 \pmod 3$.

(a) Reflections with $L = 0, \pm 1 \pmod 2$ are broadened. These correspond to the positions for the 2H structure.

(b) There are changes in the integrated intensities of different reflections.

(c) For small values of $\alpha(\alpha = 0{\cdot}02\text{–}0{\cdot}06)$ the 2H reflections remain sharp and the new 6H peaks appear as β increases to a value between 0·4 and 0·6. The 6H peaks which are initially broad become sharper as β increases to 0·9. For this range the resulting final structure shows considerable intensity at the 2H positions in comparison with the intensity at the 6H positions. The final resultant structure ($\beta = 0{\cdot}9$) shows the co-existence of the 2H and the 6H structures.

(d) For $\alpha = 0{\cdot}1$ to 0·2. The 2H reflections are broad and the new 6H peaks start appearing when $\beta = 0{\cdot}4$. The 6H peaks at $L = \pm\frac{1}{3}, \pm\frac{2}{3} \pmod 2$ are shifted away from each other. As β increases these 6H peaks gradually move from the shifted positions to the positions $L = \pm\frac{1}{3}, \pm\frac{2}{3} \pmod 2$ and all the reflections become sharper.

(e) For $\alpha = 0{\cdot}3\text{–}0{\cdot}4$. The 2H reflections are heavily broadened with a dip in the middle of the reflection. When β increases to 0·4 each reflection splits into three and as β increases above 0·4 two of them move away from the central peak to the normal 6H positions.

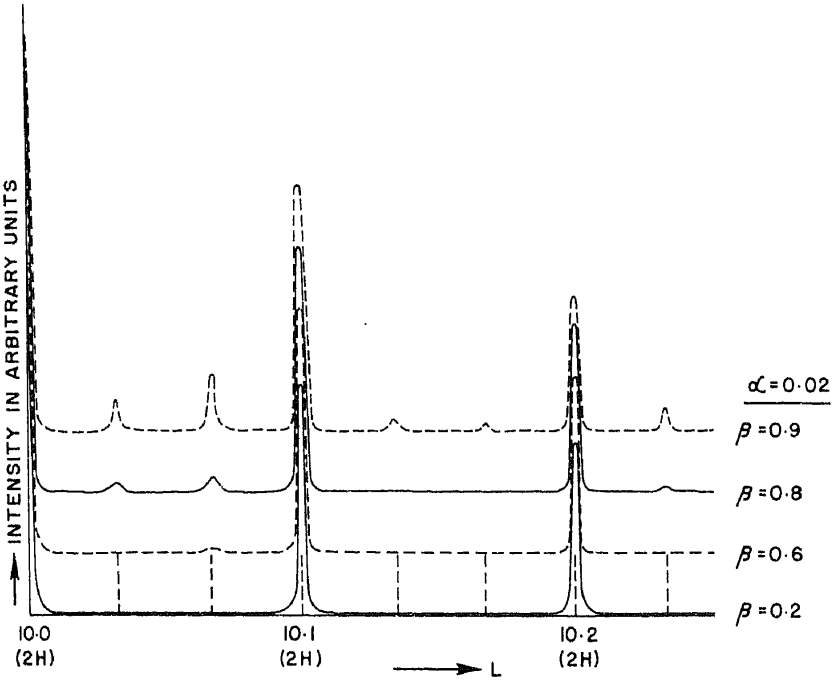

Figure 6(a).

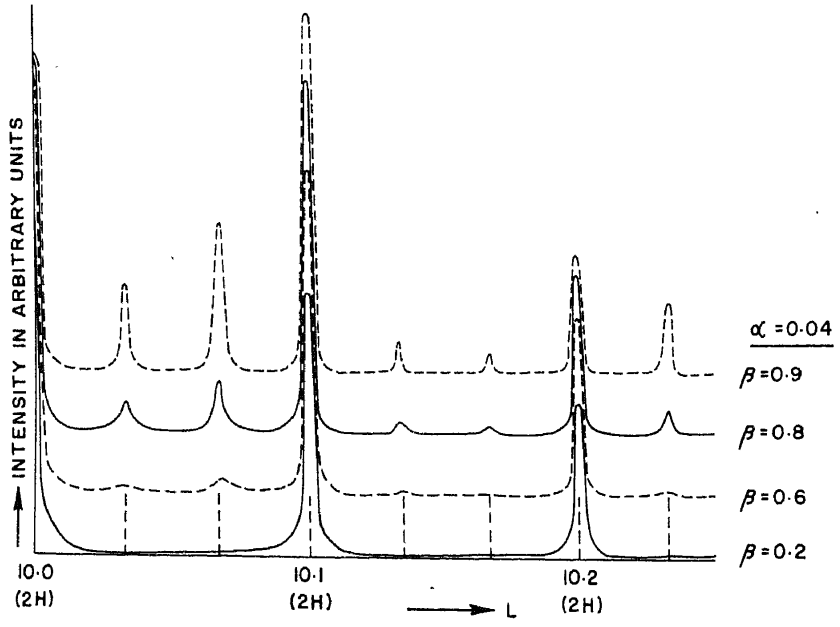

Figure 6(b).

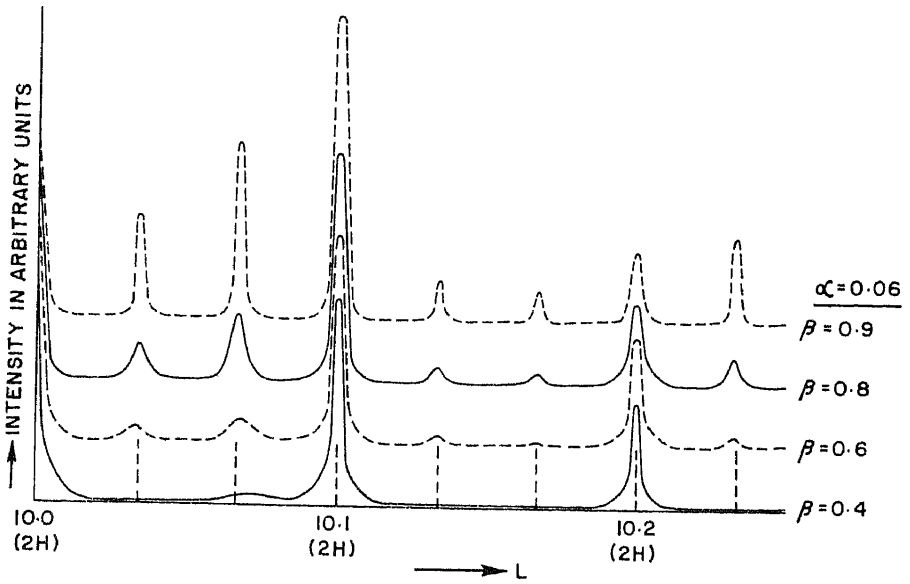

Figure 6(c).

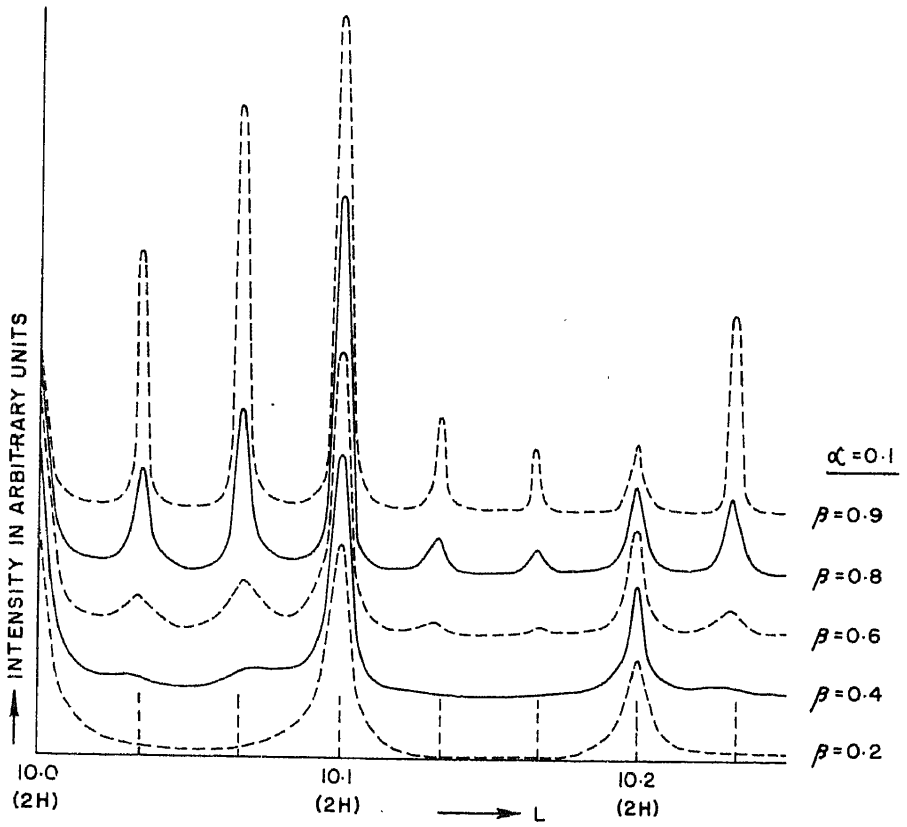

Figure 6(d).

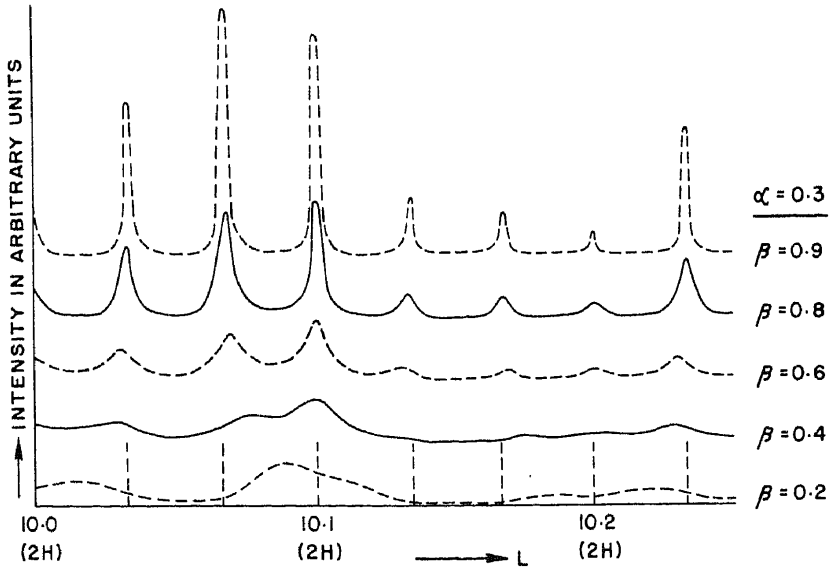

Figure 6(e).

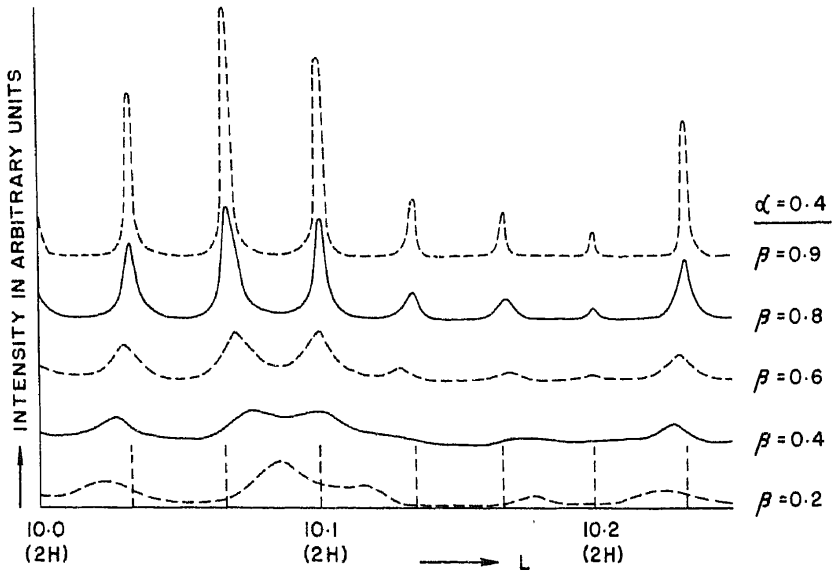

Figure 6(f).

Figure 6. Calculated variation of the diffracted intensity along the $10 \cdot L$ reciprocal lattice row for a crystal undergoing transformation by the deformation mechanism with $\beta = 0{\cdot}2, 0{\cdot}4, 0{\cdot}6, 0{\cdot}8$ and $0{\cdot}9$. The dashed vertical lines indicate the correct 6H positions. The calculated curves have been shifted vertically for different values of β for clarity. (**a**) $\alpha = 0{\cdot}02$, (**b**) $\alpha = 0{\cdot}04$, (**c**) $\alpha = 0{\cdot}06$, (**d**) $\alpha = 0{\cdot}1$, (**e**) $\alpha = 0{\cdot}3$, (**f**) $\alpha = 0{\cdot}4$.

5.2 *The theory of x-ray diffraction from 2H crystals undergoing solid state transformation to the 6H structure by the layer displacement mechanism*

Employing the notation described in the previous section the probability tree for the layer displacement mechanism can be written as follows for the two-parameter model

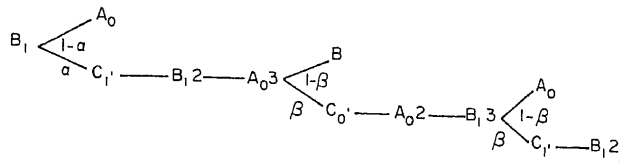

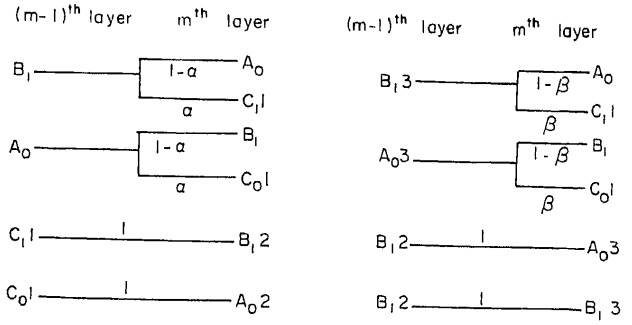

To compute the probability $P_{(m,j)}$ of arriving at the mth layer with the subscript $j(j = 0, 1, 0^1, 1^1, 0^2, 1^2, 0^3$ and $1^3)$ with the help of the probability trees, we consider the transitions from the $(m-1)$th layer to the mth layer starting with each type of layer (*i.e.* $0, 1, 0^1, 1^1, 0^2, 1^2, 0^3$ and 1^3) at the origin. Thus we have

$$
\begin{aligned}
P_{(m,0)} &= (1-\alpha)P_{(m-1,1)} + (1-\beta)P_{(m-1,1^3)},\\
P_{(m,1)} &= (1-\alpha)P_{(m-1,0)} + (1-\beta)P_{(m-1,0^3)},\\
P_{(m,0^1)} &= \alpha P_{(m-1,0)} + \beta P_{(m-1,0^3)},\\
P_{(m,1^1)} &= \alpha P_{(m-1,1)} + \beta P_{(m-1,1^3)},\\
P_{(m,0^2)} &= P_{(m-1,0^1)},\ P_{(m,1^2)} = P_{(m-1,1^1)},\ P_{(m,0^3)} = P_{(m-1,1^2)},\\
P_{(m,1^3)} &= P_{(m-1,0^2)}.
\end{aligned}
$$

Following the procedures described earlier for the deformation mechanism we get the following difference equations

$$J_{(m,0)} = (1-\alpha)J_{(m-1,1)}\omega_2 + (1-\beta)J_{(m-1,1^3)}\omega_2, \tag{26}$$

$$J_{(m,1)} = (1-\alpha)J_{(m-1,0)}\omega_1 + (1-\beta)J_{(m-1,0^3)}\omega_1, \tag{27}$$

$$J_{(m,0^1)} = \alpha J_{(m-1,0)}\omega_2 + \beta J_{(m-1,0^3)}\omega_2, \tag{28}$$

$$J_{(m,1^1)} = \alpha J_{(m-1,1)}\omega_1 + \beta J_{(m-1,1^3)}\omega_1, \tag{29}$$

$$J_{(m,0^2)} = J_{(m-1,0^1)}\omega_1, \tag{30}$$

$$J_{(m,1^2)} = J_{(m-1,1^1)}\omega_2, \tag{31}$$

$$J_{(m,0^3)} = J_{(m-1,1^2)}\omega_2, \tag{32}$$

$$J_{(m,1^3)} = J_{(m-1,0^2)}\omega_1. \tag{33}$$

Let the solution of the system of difference equations (26) to (33) be of the form

$$J_{(m,j)} = C_j \rho^m \qquad m \geqslant 0. \tag{34}$$

Substituting this value of $J_{(m,j)}$ in (26) to (33) and eliminating the various C's we finally obtain the characteristic equation

$$\rho^8 - (1-\alpha)^2 \rho^6 - 2\alpha(1-\beta)\rho^4 - \beta^2\rho^2 + (\alpha-\beta)^2 = 0. \tag{35}$$

Adopting the method described earlier we get from the probability tree

$$\begin{aligned} W_0 &= (1-\alpha) W_1 + (1-\beta) W_{1^3}, \\ W_1 &= (1-\alpha) W_0 + (1-\beta) W_{0^3}, \\ W_{0^1} &= \alpha W_0 + \beta W_{0^3} = W_{0^2} = W_{1^3}, \\ W_{1^1} &= \alpha W_1 + \beta W_{1^3} = W_{1^2} = W_{0^3}. \end{aligned}$$

But $W_0 + W_1 + W_{0^1} + W_{1^1} + W_{0^2} + W_{1^2} + W_{0^3} + W_{1^3} = 1.$

Solving the above equations we get

$$W_0 = W_1 = \frac{1-\beta}{2-2\beta+6\alpha},$$

$$W_{0^1} = W_{1^1} = W_{0^2} = W_{1^2} = W_{0^3} = W_{1^3} = \frac{\alpha}{2-2\beta+6\alpha}.$$

Proceeding in the manner described earlier for the deformation mechanism, we get the following boundary conditions

$$T_0 = 1, \quad T_1 = -\frac{1}{2}, \quad T_2 = \frac{2-2\beta}{2-2\beta+6\alpha},$$

$$T_3 = -\frac{1-\beta+3\alpha-3\alpha\beta}{2-2\beta+6\alpha}, \quad T_4 = \frac{2-2\beta+6\alpha^2-6\alpha^2\beta}{2-2\beta+6\alpha},$$

$$T_5 = -\frac{1-\beta+3\alpha-3\alpha^2+3\alpha^3+3\alpha^2\beta-3\alpha^3\beta}{2-2\beta+6\alpha},$$

$$T_6 = \frac{2-2\beta+6\alpha^2-12\alpha^3+6\alpha^4-6\alpha^2\beta+12\alpha^3\beta-6\alpha^4\beta+6\alpha\beta^2}{2-2\beta+6\alpha},$$

$$T_7 = -\frac{1-\beta+3\alpha-3\alpha^2+9\alpha^3-9\alpha^4+3\alpha^5-3\alpha^2\beta-9\alpha^3\beta+9\alpha^4\beta-3\alpha^5\beta+6\alpha^2\beta^2}{2-2\beta+6\alpha}.$$

The applicability of Holloway's method is restricted by the condition that none of the roots of the characteristic equation has unit modulus. In the present case two of the roots have unit modulus as shown below.

Equation (35) can be written as

$$(\rho^2-1)[\rho^6 + (2\alpha-\alpha^2)\rho^4 + (-\alpha^2+2\alpha\beta)\rho^2 + (-\alpha^2+2\alpha\beta-\beta^2)] = 0. \tag{36}$$

Therefore two of the roots have unit modulus *i.e.*

$$\rho_6 = 1 \text{ and } \rho_7 = -1,$$

and $a_6 = 1,\ a_4 = 2\alpha - \alpha^2,\ a_2 = -\alpha^2 + 2\alpha\beta,$

$a_0 = -\alpha^2 + 2\alpha\beta - \beta^2,\ a_5 = a_3 = a_1 = 0.$

Recently Lele (1980) obtained an analytical solution for the diffuse diffracted intensity when the characteristic equation found from the difference equation has roots with unit modulus. In this method we obtain a self-consistent set consisting of the characteristic equation and the boundary conditions which do not have the effect of any roots with unit modulus and thus can be used as input for the calculation of the diffracted intensity by Holloway's method. The diffracted intensity corresponding to the roots with unit modulus consists of sharp peaks and has to be superposed on the diffuse intensity corresponding to the roots with non-unit modulus.

Multiplying the terms inside the square bracket (36) with $(\rho+1)$ and $(\rho-1)$ respectively we get

$$\rho^7 + \rho^6 + (2\alpha - \alpha^2)\rho^5 + (2\alpha - \alpha^2)\rho^4 + (-\alpha^2 + 2\alpha\beta)\rho^3 + (-\alpha^2 + 2\alpha\beta)\rho^2 + (-\alpha^2 + 2\alpha\beta - \beta^2)\rho + (-\alpha^2 + 2\alpha\beta - \beta^2) = 0, \tag{37}$$

and

$$\rho^7 - \rho^6 + (2\alpha - \alpha^2)\rho^5 - (2\alpha - \alpha^2)\rho^4 + (-\alpha^2 + 2\alpha\beta)\rho^3 - (-\alpha^2 + 2\alpha\beta)\rho^2 + (-\alpha^2 + 2\alpha\beta - \beta^2)\rho - (-\alpha^2 + 2\alpha\beta - \beta^2) = 0. \tag{38}$$

From (37) and (38) we get the following coefficients

$$b_6 = 1,\ b_5 = 2\alpha - \alpha^2,\ b_4 = 2\alpha - \alpha^2,\ b_3 = -\alpha^2 + 2\alpha\beta,\ b_2 = -\alpha^2 + 2\alpha\beta,$$
$$b_1 = -\alpha^2 + 2\alpha\beta - \beta^2,\ b_0 = -\alpha^2 + 2\alpha\beta - \beta^2,$$
$$b'_6 = -1,\ b'_5 = 2\alpha - \alpha^2,\ b'_4 = -(2\alpha - \alpha^2),\ b'_3 = (-\alpha^2 + 2\alpha\beta),$$
$$b'_2 = -(-\alpha^2 + 2\alpha\beta),\ b'_1 = -\alpha^2 + 2\alpha\beta - \beta^2,\ b'_0 = -(-\alpha^2 + 2\alpha\beta - \beta^2).$$

Following Lele (1980),

$$C_0 = \frac{T_{m-1} + b_{n-2}T_{n-2} \ldots + b_1 T_1 + b_0 T_0}{\rho_0^{n-1} + b_{n-2}\rho_0^{n-2} \ldots + b_1\rho_0 + b_0},$$

we get

$$C_6 = \frac{T_7 + b_6 T_6 + \ldots + b_0 T_0}{\rho_6^7 + b_6\rho_6^6 \ldots + b_1\rho_6 + b_0}.$$

Substituting the values of T's and b's and $\rho_6 = 1$ we get

$$C_6 = \frac{1 - \alpha - \beta - \beta^2 + \beta^3 - \alpha\beta^2 + 2\alpha\beta}{4(1 - \beta + 3\alpha)(1 + 2\alpha + 4\alpha\beta - 3\alpha^2 - \beta^2)}.$$

Similarly,

$$C_7 = \frac{T_7 + b'_6 T_6 + \ldots + b_{1'} T_1 + b'_0 T_0}{\rho_7^7 + b'_6\rho_7^6 + \ldots + b'_1\rho_7 + b'_0}$$
$$= \frac{3 - 3\beta + 9\alpha - 3\beta^2 + 6\alpha\beta - 15\alpha\beta^2 + 24\alpha^2\beta - 12\alpha^3 + 3\beta^3}{4(1 - \beta + 3\alpha)(1 + 2\alpha + 4\alpha\beta - 3\alpha^2 - \beta^2)}.$$

The boundary conditions which no longer have the effects of any roots with unit modulus are given by

$$K_m = T_m - \sum_{j=n-p}^{n-1} C_j \rho_j^m,$$

where the roots, ρ_j, $j = (n-p)$ to $(n-1)$ have unit modulus. Thus we have

$$K_1 = T_1 - (C_6\rho_6 + C_7\rho_7) = T_1 - (C_6 - C_7)$$
$$K_2 = T_2 - (C_6 + C_7), \quad K_3 = T_3 - (C_6 - C_7),$$
$$K_4 = T_4 - (C_6 + C_7), \quad K_5 = T_5 - (C_6 - C_7).$$

Substituting the five boundary conditions (K's) and the coefficients (a's) of the characteristic equation in Holloway's expression

$$I = f^2C\left\{\left[\frac{1}{2} + \frac{\sum_{j=1}^{n-1}\sum_{p=0}^{j-1} a_{n-p}K_{j-p}\exp(n-j)i\pi L - a_0}{\sum_{j=0}^{n} a_j \exp(ji\pi L)}\right] + \text{C.C.}\right\},$$

where C.C. stands for the complex conjugate, we get

$$I = f^2C\{(\tfrac{1}{2} + [K_1\exp(5i\pi L) + K_2\exp(4i\pi L) + (K_3 + a_4K_1)\exp(3i\pi L) + (K_4 + a_4K_2)\exp(2i\pi L) + (K_5 + a_4K_3 + a_2K_1)\exp(i\pi L) - a_0]/(a_0 + a_2\exp(2i\pi L) + a_4\exp(4i\pi L) + \exp(6i\pi L))) + \text{C.C.}\}$$

On simplifying we get the final intensity expression for a 2H crystal undergoing solid state transformation to the 6H structure by the layer displacement mechanism as

$$I = f^2C\left(1 + \frac{x}{y}\right), \tag{39}$$

where

$$x = B_1R_1 + a_4B_1R_1 + a_2B_1R_3 + a_0B_1R_5 + B_2R_2 + a_4B_2 + a_2B_2R_2 + a_0B_2R_4 + B_3R_3 + a_4B_3R_1 + a_2B_3R_1 + a_0B_3R_3 + B_4R_4 + a_4B_4R_2 + a_2B_4 + a_0B_4R_2 + B_5R_5 + a_4B_5R_3 + a_2B_5R_1 + a_0B_5R_1 + B_6R_6 + a_4B_6R_4 + a_2B_6R_2 + a_0B_6,$$

$$y = 1 + a_0^2 + a_2^2 + a_4^2 + 2a_0a_2R_2 + 2a_0a_4R_4 + 2a_0R_6 + 2a_2a_4R_2 + 2a_2R_4 + 2a_4R_2.$$

$$B_1 = 2K_1, \quad R_1 = \cos\pi L,$$
$$B_2 = 2K_2, \quad R_2 = \cos 2\pi L,$$
$$B_3 = 2(K_3 + a_4K_1), \quad R_3 = \cos 3\pi L,$$
$$B_4 = 2(K_4 + a_4K_2), \quad R_4 = \cos 4\pi L,$$
$$B_5 = 2(K_5 + a_4K_3 + a_2K_1), \quad R_5 = \cos 5\pi L,$$
$$B_6 = -2a_0, \quad R_6 = \cos 6\pi L.$$

5.2a *Prediction of diffraction effects.* The variation of the diffracted intensity along the $10 \cdot L$ reciprocal lattice row for different values of α and β (calculated from (39) in steps of $\Delta L = 0{\cdot}01$) is depicted in figure 7a, b, c. The intensity corresponding to roots with unit modulus consists of sharp peaks and has to be superposed on the diffuse intensity shown in the figure. The diffraction effects from 2H crystals undergoing transformation

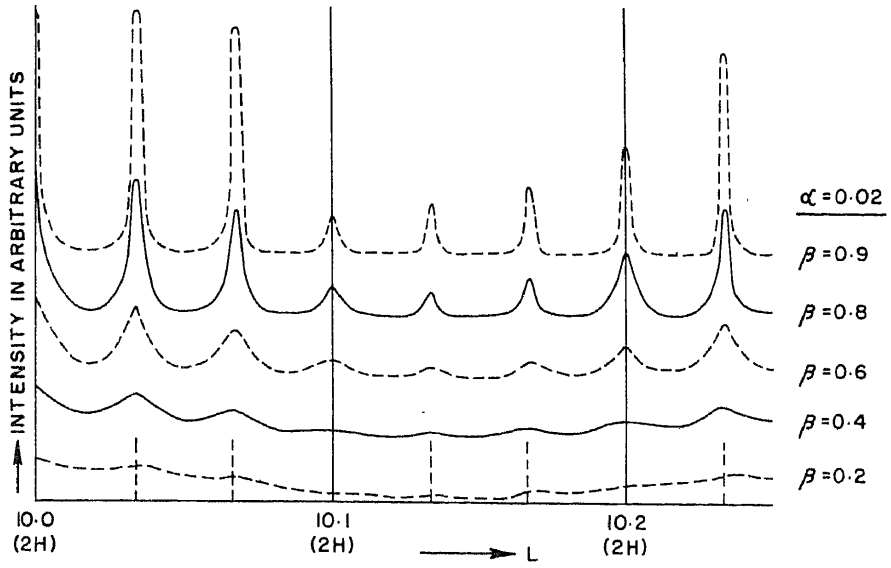

Figure 7(a).

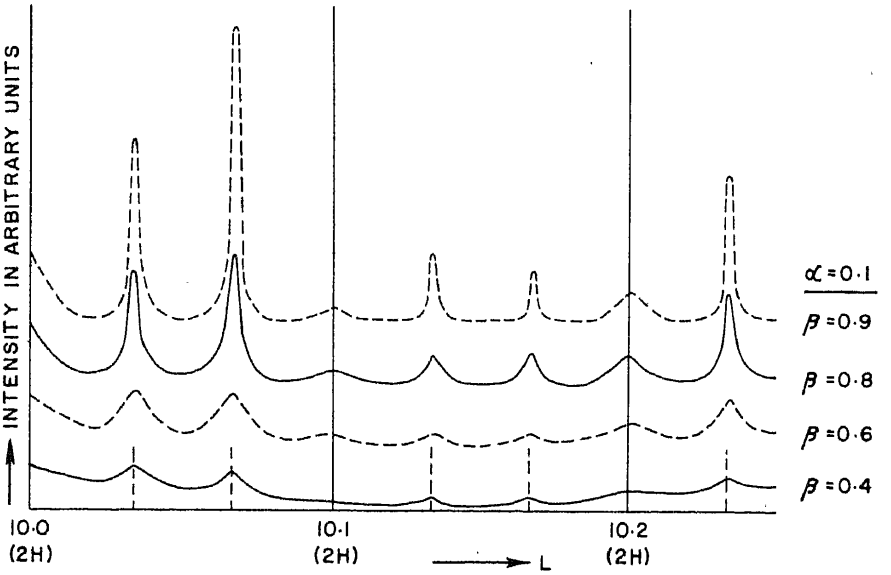

Figure 7(b).

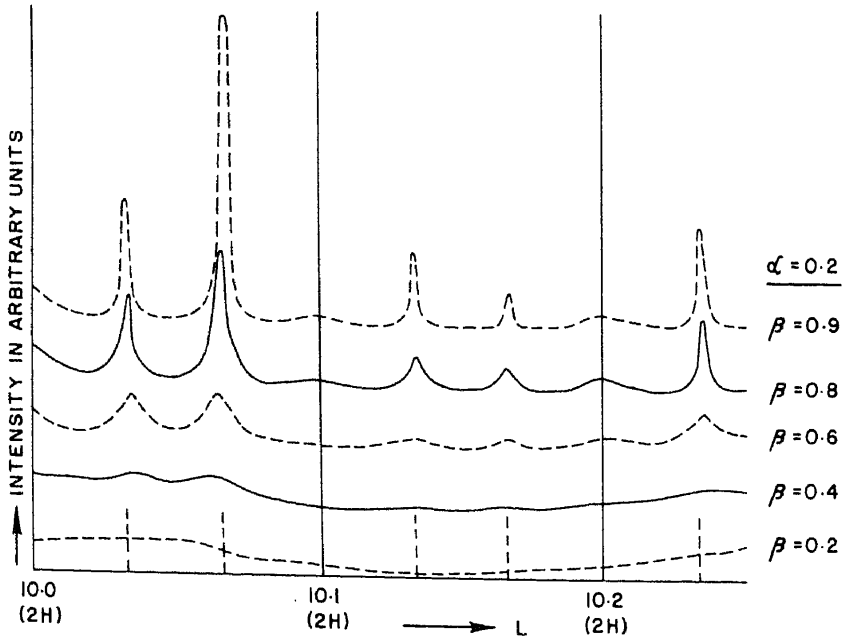

Figure 7(c).

Figure 7. Calculated variation of the diffracted intensity along the $10 \cdot L$ reciprocal lattice row for a crystal undergoing transformation by the layer displacement mechanism with β = 0·2, 0·4, 0·6, 0·8 and 0·9. The dashed vertical lines indicate the correct 6H positions. The calculated curves have been shifted vertically for different values of β for clarity. (a) α = 0·02, (b) α = 0·1, (c) α = 0·2.

to the 6H structure by the layer displacement mechanism may be summarised as follows

(i) The reflections with $H - K = 0$ (mod 3) and $L = 0$ (mod 2) are unaffected by the transformation and remain sharp throughout the transformation.

(ii) The following diffraction effects are predicted for the reflections with $H - K \neq 3n$

(a) reflections with $L = 0, \pm 1$ (mod 2) are not broadened,

(b) There are changes in the integrated intensities of the different reflections.

(c) For α = 0·02 to 0·1: The new 6H peaks appear at $L = \pm\frac{1}{3}, \pm\frac{2}{3}$ (mod 2) when β increases to a value of about 0·2. Initially these reflections are broad and as β increases to 0·9 they become sharper.

(d) For α = 0·2 to 0·4: When β = 0·2 new heavily broadened peaks appear at $L = \pm\frac{1}{2}$ (mod 2). When β increases to a value between 0·4 and 0·6 these peaks broaden and split into two. As β increases to a still larger value (0·6–0·9) these reflections which have split into two peaks move away from each other towards the normal 6H positions, viz. $L = \pm\frac{1}{3}, \pm\frac{2}{3}$ (mod 2) and become sharper.

(e) The 2H peaks are present throughout the transformation as in the case of deformation mechanism. The one-parameter model does not show such a co-existence of 2H and 6H peaks.

6. Comparison of theoretically predicted diffraction effects with those experimentally observed

A study of the x-ray photographs and the corresponding intensity profiles of the crystals in different stages of the transformation shows that the transformation commences with a broadening of the 2H reflections. This broadening is small when α is small but quite considerable for larger values of α. The experimentally obtained intensity profiles (diffractometer records of intensity) approximate to the theoretical profiles computed for the deformation mechanism. In many crystals the new 6H peaks are observed to be shifted away from each other at the initial stages of transformation in accordance with the predictions of the deformation mechanism. For transformation by the layer displacement mechanism the 2H reflections would have remained sharp and the new 6H peaks would be shifted towards each other in partially transformed crystals. The range of α and β values for two typical crystals obtained by comparing the experimental profiles (figures 4 and 5) with the theoretically calculated profiles for the deformation mechanism are

$\alpha = 0{\cdot}06$–$0{\cdot}1$, $\beta = 0{\cdot}6$–$0{\cdot}8$ (figure 4),
$\alpha = 0{\cdot}06$–0.1, $\beta = 0{\cdot}8$–$0{\cdot}9$ (figure 5).

7. Discussion of results

It is found that the phenomena of polytypism and one-dimensional disorder cease to occur in $Zn_xCd_{1-x}S$ crystals for $x < 0{\cdot}94$. Only perfect 2H structure occurs for $x \leqslant 0{\cdot}93$. This is in agreement with earlier studies performed on melt grown crystals (Kozielski 1976). A higher cadmium content stabilizes the 2H phase. Similar studies performed with ZnS and ZnSe which form solid solutions of the type $ZnS_{1-x}Se_x$ over the entire composition range from $x = 0$ to 1, have shown (Kozielski 1976) that polytypes and disordered structures occur only in the range $0 < x < 0{\cdot}3$. The hexagonality of the crystals increases with increasing selenium content. Melt grown solid solutions of the type $ZnS_{1-x}Te_x$ are also known to display (Kozielski 1976) polytypes and one-dimensional disordered structures. Apparently in all these systems the stacking fault energy (SFE) is a function of composition and disorder effects cease when SFE becomes greater than a certain critical value.

It is known (Sebastian *et al* 1982) that 2H ZnS transforms to a disordered twinned 3C structure on annealing and that deformation faults nucleate the transformation. Shachar *et al* (1968) have reported that the 2H ZnS crystals transform to a disordered 3C + 6H structure on applying external stresses by a needle or a knife edge. Consequently it is expected that deformation faults are also involved in the 2H–6H solid state transformation observed in $Zn_xCd_{1-x}S$ and $Zn_xMn_{1-x}S$ crystals. The transformations occur by the non-random insertion of deformation faults but the one-parameter model developed (Pandey *et al* 1980) for a similar transformation in SiC is not applicable to these materials. The two-parameter model described above does explain the observed intensity distribution approximately for $\beta \gg \alpha$. The peak shift and peak broadening of the reflections with $H - K \neq 3n$ depend on the relative magnitudes of α and β. The partially transformed $Zn_xCd_{1-x}S$ and $Zn_xMn_{1-x}S$ crystals are found to possess a small value of α ($\alpha = 0{\cdot}02$ to $0{\cdot}2$) and a large value of β ($\beta = 0{\cdot}4$ to $0{\cdot}9$) during

the 2H–6H transformation. This implies that the 2H–6H transformation in these materials commences with the random insertion of a few deformation faults (small α) which quickly develop into 6H nuclei by preferred faulting at 3-layer separations (large β). For larger values of α the reflections with $H-K \neq 3n$ and $L = \pm\frac{1}{3}, \pm\frac{2}{3}$ will become broadened and show peak shifts. The case when $\alpha = \beta$ corresponds to the one-parameter model developed by Pandey *et al* (1980). For $\alpha \ll \beta$, a small number of 6H nuclei would grow into thick 6H regions. Therefore the 6H reflections would appear at an early stage of transformation and the 2H reflections will not broaden considerably. This is what we observe in the case of the 2H–6H transformation in $Zn_xCd_{1-x}S$ and $Zn_xMn_{1-x}S$.

The diffractometer records in figure 5 show an enhancement of intensity at 3C positions which is observed in many crystals. It indicates that there is a finite probability of faults occurring also at two-layer separations. The assumption that the probability of faulting at less than three-layer separations is zero, is therefore an approximation and the actual faulting in such a system is more complicated.

Acknowledgements

The authors are grateful to the Department of Science and Technology, New Delhi, for providing financial assistance. Thanks are also due to Dr S Lele for helpful discussions. One of us (PK) is grateful to Prof. H Schulz for providing single crystal diffractometer facilities at the Max-Planck Institute (FKF), Stuttgart, W. Germany.

References

Brodin M S, Budnik P I, Vitrikhoski N I and Zakreveskii S V 1970 *Sov. Phys. Semiconductors* **4** 435
Burton L C and Hench T L 1976 *Appl. Phys. Lett.* **29** 612
Chandrasekharaiah M N and Krishna P 1969 *J. Cryst. Growth* **5** 213
Cherin P, Lind E L and Davies E A 1970 *J. Electrochem. Soc.* **117** 233
Daniels B K 1966 *Philos. Mag.* **14** 487
Domeus P, Cadene M, Cohen C W and Martinuzzi S 1977 *Photovoltaic solar energy conversion, Proc. Conf., Luxemburg*, p. 168
Holloway H 1969 *J. Appl. Phys.* **40** 4313
Inouguchi T, Takeda M, Kakihara Y and Yoshira M 1974 *Stable high luminescence thin film electroluminescent panels in Dig. SID Int. Symp., Los Angeles, CA. Soc. for Inf. Disp.* p. 86
Jagodzinski H 1949 *Acta Crystallogr.* **2** 208
Juza V R, Rabenau A and Pascher G 1956 *Z. Anorg. Allg. Chem.* **285** 611
Kawaguchi H, Ito H and Inaba H 1976 *Opt. Commun.* **16** 6
Kozielski M J 1976 *J. Cryst. Growth* **30** 86
Krishna P and Marshall R C 1971 *J. Cryst. Growth* **9** 319, *ibid* **11** 147
Kröger F A 1939 *Z. Kristallogr.* **A 100** 132 *ibid* 543
Lele S 1980 *Acta Crystallogr.* **A36** 584
Lele S and Pandey D 1982 *Proc. Int. Conf. on Solid to solid phase transformations. AIME Warandale*, p. 1487
Lutz H P and Becker W 1977 *J. Solid State Chem.* **20** 183
Mardix S and Steinberger I T 1966 *Isr. J. Chem.* **3** 243
Mehmed F and Heraldson H 1938 *Z. Anorg. Chem.* **235** 193
Müller H 1952 *News Jahrb. Miner. Abh.* **84** 43
Pandey D and Krishna P 1977 *J. Phys.* **D10** 2057
Pandey D, Lele S and Krishna P 1980 *Proc. R. Soc. (London)* **A369** 435, 451, 463
Prasad B and Lele S 1971 *Acta Crystallogr.* **27** 54

Roomians C J M 1963 *J. Inorg. Nucl. Chem.* **25** 253
Schnaase H 1933 *Z. Phys. Chem.* **B20** 89
Sebastian M T, Pandey D and Krishna P 1982 *Phys. Status Solidi* **71** 633
Sebastian M T and Krishna P 1983 *Solid State. Commun.* **48** 879
Sebastian M T and Krishna P 1983a *Bull. Mater. Sci.* **5** 257
Sebastian M T and Krishna P 1983b *Phys. Status Solidi* **79** 271
Secco d'Aragona F S, Delavignette P and Amelinckx S 1966 *Phys. Status Solidi* **K14** 115
Shachar G, Mardix S and Steinberger I T 1968 *J. Appl. Phys.* **39** 2485
Singer J 1963 *Acta Crystallogr.* **16** 601
Theis D 1981 *J. Lumines.* **23** 191
Yoshikawa A and Sakai Y 1976 *Jpn. J. Appl. Phys.* **15** 1861